第35卷第5期
2016年10月

红外与毫米波学报
J. Infrared Millim. Waves

Vol. 35, No. 5
October, 2016

文章编号: 1001 - 9014(2016)05 - 0529 - 05

DOI:10.11972/j.issn.1001 - 9014.2016.05.004

Ka-band wideband power amplifier MMIC using capacitive coupled matching structure

LIN Hao-Dong[1*], LIU Yu[1], DONG Jun[2], YUAN Ye[1], YANG Tao[1], XIE Xiao-Qiang[1]

(1. School of Electronic Engineering, University of Electronic Science and Technology of China, Chengdu 611731, China;
2. College of Physics and Information Science, Hunan Normal University, Changsha 410081, China)

Abstract: Adopting the capacitive coupled matching structure, a Ka-band wideband three-stage power amplifier (PA) MMIC was designed by 0.1μm GaAs pHEMT process in this paper. To facilitate the design of wideband PA, a set of formulas was proposed to analyze this matching structure. This structure achieves wide operating band and high power-added efficiency (PAE) simultaneously in the presented PA. The measured saturation PAE is upon 30% over 32 ~ 40 GHz with 20 dBm output power and more than 15.5 dB power gain, which demonstrates the effectiveness of this design skill.

Key words: coupled resonator matching, wideband power amplifier, gigh efficiency, ka-Band, MMIC
PACS: 84.30.Le, 84.40.Dc

基于容性耦合匹配结构的 Ka 波段宽带功放 MMIC

林浩冬[1*], 刘 宇[1], 董 俊[2], 袁 野[1], 杨 涛[1], 谢小强[1]

(1. 电子科技大学 电子工程学院,四川 成都 611731;
2. 湖南师范大学 物理与信息科学学院,湖南 长沙 410081)

摘要:采用容性耦合匹配结构,基于0.1μm GaAs pHEMT工艺设计了一个Ka波段三级宽带功率放大器MMIC.为了辅助宽带功放设计,提出了一组公式来分析这一匹配结构.在展示的功放中,此结构同时实现了宽频带和高效率.功放处于饱和状态时,测得在32 ~ 40 GHz频率范围内的PAE大于30%,功率增益超过15.5 dB,功率约20 dBm.这一结果证明了这种设计方法的有效性.

关 键 词:耦合谐振器匹配;宽带功放;高效率;Ka波段;MMIC

中图分类号:TN722.1+6,TN952 **文献标识码**:A

Introduction

The demands for high ranging resolution and imaging accuracy of radar have motivated the need for wideband wireless front-end[1]. The wideband power amplifier (PA) is the key component of front-end. The output matching of PA is the most significant to its performance. The two most commonly used wideband matching topologies (inductive coupled matching and capacitive coupled matching) can be analyzed by coupled resonator theory. The analysis of inductive coupled matching (i-matching) was proposed in[2] with a wideband PA for verification. However, the bandwidth of i-matching is limited by the parasitic drain inductor (presenting high reactance at the high band of millimeter wave). This bandwidth limitation can be solved by a lossy i-matching with embedded resistor[3], but it is only suitable for low noise amplifier not for PA.

In this paper, the different operation mechanism of capacitive coupled matching (c-matching) is also explained by coupled resonator theory. The comparison indicates that c-matching can overcome the bandwidth limitation of i-matching at the high band of millimeter wave. Besides, to facilitate the design of wideband PA with c-matching topology, a set of formulas were derived to calculate its initial values for optimization.

For verification, a three-stage 100 mW medium PA

Received date: 2016-03-15, **revised date**: 2016-06-29 **收稿日期**:2016-03-15, **修回日期**:2016-06-29
Foundation items:The project is supported by National Natural Science Foundation of China (61271034)
Biography:LIN Hao-Dong (1982-), male, Sichuan, China, Ph. D Candidate. Research fields are RF, microwave, millimeter-wave circuits and systems. E-mail: harry19820206@outlook.com
* **Corresponding author**:E-mail:harry19820206@outlook.com

monolithic microwave integrated circuit (MMIC) with the c-matching structure was presented. This PA chip achieves 30 ~ 35.5% saturation power-added efficiency (PAE) over the bandwidth of 32 ~ 40 GHz. To our knowledge, this PA has the highest PAE lower-bound (30%) in Ka-band multi-stage wideband (fractional bandwidth >20%) PA chips[4-9].

1 Capacitive coupled matching technique

The i-matching is shown in Fig. 1(a). The output impedance of transistor (denoted as Z_{ds}) is composed of R_{ds}, C_{ds} and L_d (R_{ds} and C_{ds} are the intrinsic elements between drain and source, L_d is the parasitic inductor of drain). The mutual inductor of L_1 and L_2 is L_M. L_d plays a part of L_1. Z_0 presents the 50 Ω load impedance. The resonator1 contains C_{ds} and L_1, while resonator2 contains L_2 and C_1. Correspondingly, as shown in Fig. 1(b), L_d of c-matching is a part of L_3. And T-T' means a reference plane. The resonator3 is composed of C_{ds}, L_3, and C_M. The resonator4 is composed of C_M, L_4, and C_2.

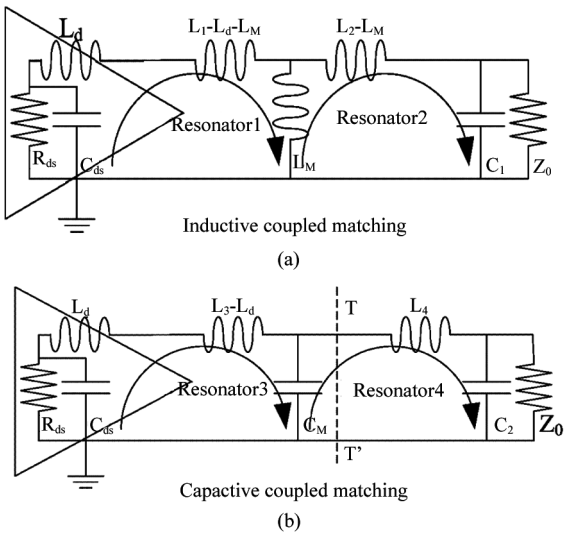

Fig. 1 (a) Inductive and (b) capacitive coupled matching
图1 (a) 感性耦合匹配. (b) 容性耦合匹配

The coupling coefficient of i-matching can be calculated by Eq. (1)[2].

$$k_m = L_M / \sqrt{L_1 L_2} \quad . \quad (1)$$

Similarly, the coupling coefficient of c-matching (k_e) can be expressed as Eq. (2), which assumes that the currents of resonator3 and resonator4 are I_3 and I_4, respectively. And Eq. (3) is simplified from Eq. (2).

$$k_e = (0.5|I_3||I_4|/j\omega C_M)/[(0.5|I_3|^2/j\omega C_M + 0.5|I_3|^2/j\omega C_{ds}) \times (0.5|I_4|^2/j\omega C_M + 0.5|I_4|^2/j\omega C_2)]^{1/2} \quad , \quad (2)$$

$$k_e = \sqrt{C_{ds}C_2/[(C_M + C_{ds})(C_M + C_2)]} \quad . \quad (3)$$

To simplify the analysis, the two coupled resonators are approximately assumed to have the same self-resonant frequency. Then, the self-resonant frequency of resonator1 and resonator2 can be presented as Eq. (4)[2].

$$\omega_{0m}^2 = [L_1 C_{ds}]^{-1} = [L_2 C_1]^{-1} \quad . \quad (4)$$

As assumed above, the self-resonant frequency of resonator3 and resonator4 can be written as Eq. (5).

$$\omega_{0e}^2 = \frac{C_{ds} + C_M}{L_3 C_M C_{ds}} = \frac{C_2 + C_M}{L_4 C_M C_2} \quad . \quad (5)$$

The two unloaded resonant frequencies of inductive coupled resonators are ω_1 and ω_2 ($0 < \omega_1 < \omega_2$) in Eq. (6)[2].

$$\omega_1 = \omega_{0m}/\sqrt{1 + k_m}; \omega_2 = \omega_{0m}/\sqrt{1 - k_m} \quad . \quad (6)$$

Correspondingly, in the proposed c-matching, the unloaded resonance condition of capacitive coupled resonators can be expressed as Eq. (7), which means the susceptances without R_{ds} and Z_0 at left and right of T-T' plane are opposite sign.

$$j\omega C_M + j\omega C_{ds}/[1 - \omega^2 C_{ds} L_3] = -j\omega C_2/(1 - \omega^2 C_2 L_4) \quad . \quad (7)$$

Substituting Eq. (5) into Eq. (7), Eq. (7) can be simplified as Eq. (8).

$$\omega^2 = \omega_{0e}^2(1 \pm \sqrt{C_{ds}C_2}/(\sqrt{C_M C_{ds}} \times \sqrt{C_M C_2})) = \omega_{0e}^2(1 \pm k_e) \quad . \quad (8)$$

The two unloaded resonant frequencies (ω_3 and ω_4) of capacitive coupled resonators are the solutions of Eq. (8). Because $0 < \omega_3 < \omega_4$, Eq. (9) is gotten.

$$\omega_3 = \omega_{0e}\sqrt{1 - k_e}; \omega_4 = \omega_{0e}\sqrt{1 + k_e} \quad . \quad (9)$$

Each pair of resonant frequencies (Eq. (6 and 9)) can be approximated as the two transmission poles of coupled matching with the central operating frequency ω_{0m} or ω_{0e}. The matching bandwidth can be enlarged by increasing the coupling coefficient and separating the two resonant frequencies.

Reference [2] regards the wideband i-matching of high km as an ideal transformer ($k_m = 1$) approximately. So L_2 can be estimated from Eq. (10), which is the impedance transformation ratio of the ideal transformer.

$$Z_0/R_{ds} = L_2/L_1 \quad . \quad (10)$$

According to the above method, C_2 of c- matching can also be estimated by $k_e \approx 1$. When $C_M \approx 0$ (if C_M gets 0, Eq. (5) will fail), k_e is approximated as 1 from Eq. (3), thus the pole ω_4 is about ω_{0e} as Eq. (9). Equation (11) means impedances at left and right of T-T' plane are conjugate matched at ω_{0e} in the condition of $C_M \approx 0$.

$$j\sqrt{2}\omega_{0e}L_3 + 1/(1/R_{ds} + j\sqrt{2}\omega_{0e}C_{ds}) = (j\sqrt{2}\omega_{0e}L_4 + 1/(1/Z_0 + j\sqrt{2}\omega_{0e}C_2))^* \quad . (11)$$

From Eq. (12) which is the real part condition of Eq. (11), C_2 can be solved. C_2 is the closest element to const 50Ω load Z_0, and then the value of C_2 is not sensitive to bandwidth variation. Therefore, C_2 solved from Eq. (12) can ensure enough accuracy.

$$R_{ds}/(1 + 2\omega_{0e}^2 R_{ds}^2 C_{ds}^2) = Z_0/(1 + 2\omega_{0e}^2 Z_0^2 C_2^2) \quad . \quad (12)$$

Derived from Eqs. (1, 4, 6, 10) for i-matching and Eqs. (3, 5, 9, 12) for c-matching, all elements get approximate values, which can be used as a comparison of the two matches and set as initial values of optimization. As these element values cannot be negative, k_m

has a limited maximum as Eq. (13) (not mentioned in Ref. [2]). Thus the maximum bandwidth of i-matching decreases along with the increase of the operating frequency ω_{0m}. Differently, when the value of C_M is very small, k_e could approach 1, so the bandwidth of c-matching is not limited by the operating frequency ω_{0e}.

$$\max(k_m) = (1 - L_d C_{ds} \omega_{0m}^2) \sqrt{R_{ds}/Z_0} \quad . \quad (13)$$

In above analysis, the loaded resonators are approximated as unloaded, so there will be some frequency offset in these values calculated from Eqs. (1, 3-6, 9, 10, 12). To correct the frequency offset in c-matching, one solution method is introduced as following. The parallel RC is equivalent to series RC at ω_{0e} in Eq. (14). Then C_{ds} and C_2 in Eq. (5) are replaced by C_{ds_co} and C_{2_co}. This correcting method could obviously compensate the frequency offset.

$$(1/R_{ds} + j\omega_{0e} C_{ds})^{-1} = R_{ds\_co} + 1/j\omega_{0e} C_{ds\_co}$$
$$(1/Z_0 + j\omega_{0e} C_2)^{-1} = Z_{0\_co} + 1/j\omega_{0e} C_{2\_co} \quad . \quad (14)$$

The two matching structures have been analyzed and compared as above. The formulated c-matching is verified in next section. And its improvements on i-matching is also presented.

2 Wideband PA design based on capacitive coupled matching

As shown in Fig. 2, the amplifier adopts a single-end three-stage structure. With the maximized gain of first stage, the output power of second stage at 0.5dB gain compression is optimized to drive the final stage. To achieve high PAE of the whole amplifier, the final stage is tuned at 2.5 dB gain compression. This amplifier was fabricated using Win Semiconductor's pHEMT process (0.1μm gate-length with 130 GHz f_t and 180 GHz f_{max}) on 4 mil GaAs substrate[10]. The widths of the three-stage transistors are 2×25 μm, 2×50 μm, and 4×75 μm with 1:2:6 driving ratio. Moreover, the quiescent currents are 8, 17, and 49 mA with -0.5 V gate and 3 V drain bias.

The output matching of this PA was designed by the capacitive coupled matching method. The output impedance (Z_{ds}) is decided to optimize PAE of PA in the whole operating band. There are three known conditions, including the Z_{ds} of final stage (R_{ds} = 27.4 Ω, C_{ds} = 188 fF and L_d = 30 pH), the operating band of 32 GHz(ω_3) ~40 GHz(ω_4), as well as the central operating frequency ω_{0e} of 36 GHz. All element values in c-matching could be initially obtained as following. Firstly, C_2 is calculated from Eq. (12). Secondly, C_{ds} and C_2 in Eq. (5) are replaced by C_{ds_co} and C_{2_co} of Eq. (14). Thirdly, C_M is calculated from Eqs. (3, 9). Tuning the value of C_M, corresponding L_3 and L_4 are derived from the corrected Eq. (5), due to that the C_M for desired bandwidth is a little smaller than the calculated. In this case, C_M = 330 fF is a better value. So all initial values for optimization of c-matching are calculated. Finally, the calculated element values are optimized in CAD tools to achieve the best performance.

The simulated return losses of the two different

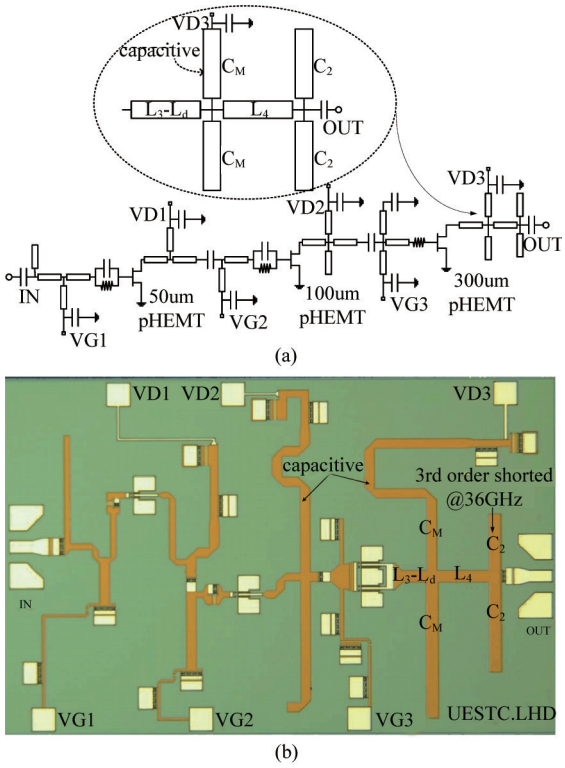

Fig. 2 (a) Schematic diagram of PA, (b) Photograph of the fabricated PA MMIC
图 2 (a) 功放原理图, (b) 功放芯片实物照片

matching methods at R_{ds} port are shown in Fig. 3(a), where the calculated and optimized results are presented simultaneously. With the agreement of calculated and optimized c-matchings, the accuracy of frequency offset correcting method as Eq. (14) is verified. Meanwhile, the calculated i-matching[2] (centered on 48 GHz) presents obvious frequency offset from optimized results. The optimized two matchings in three operating bands are shown in Fig. 3(b). It can be observed clearly that all c-matchings achieve two transmission poles while all i-matchings achieve only one. These results verify our analysis that the bandwidth of i-matching is limited by the high reactance of $j\omega_{0m} L_d$ as shown in Eq. (13). Conversely, the c-matching with two transmission poles means better wideband matching performance. The wider the band is, the more obvious the advantage of c-matching is.

As the matching goal Z_{ds} is optimized for high PAE, the matching performance could be observed from PAE. The simulated impedance tracks (optimized matchings) versus PAE contours of 0.2% step are shown in Fig. 4. The ideal impedance is conjugate Z_{ds}. The c-matching (achieving two poles) gets close to ideal impedance twice, and its PAE decrements are 0.2% at 32 GHz and 0.4% at 40 GHz in contours. Differently, the i-matching (only achieving one pole) crosses ideal impedance only once, and its PAE decrements are 1.4% at 32 GHz and 1.2% at 40 GHz. The PAE improvements of c-matching versus i-matching are 1.2% and 0.8% at the two-ends of operating band, while little difference at the middle.

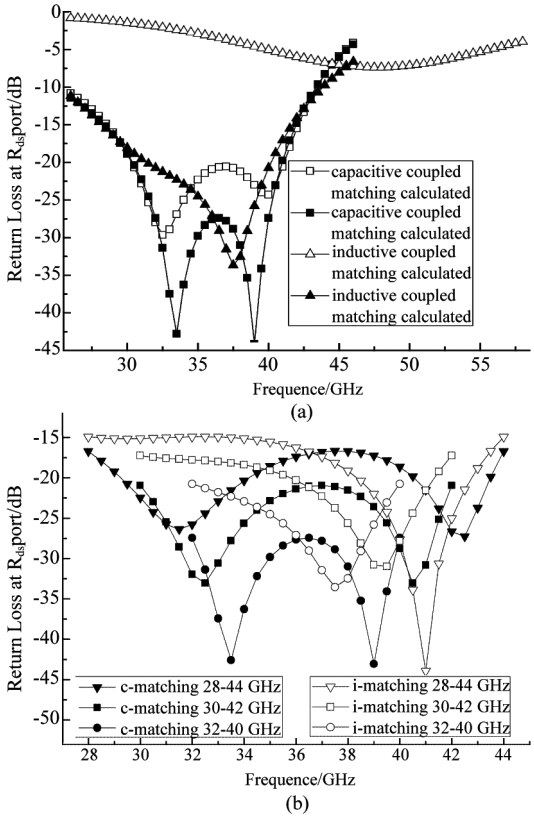

Fig. 3 (a) Calculated and optimized matchings for 32 ~ 40 GHz, (b) Optimized matchings in three operating bands
图 3 (a) 为 32 ~ 40 GHz 计算和优化的两种匹配,(b) 为 3 种工作频带优化的两种匹配

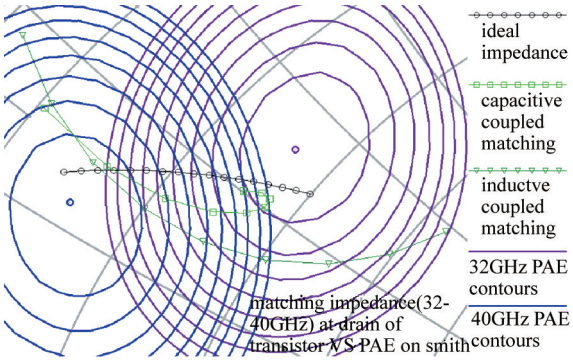

Fig. 4 Impedance tracks on load-pull smith chart
图 4 负载牵引史密斯圆图上的阻抗轨迹

The c-matching is adopted in the fabricated PA. In Fig. 2(b), C_M and C_2 are implemented by bilateral microstrip stubs, while L_3-L_d and L_4 are equivalent to microstrip lines with certain length. Because the right top stub in the output matching shorts the 3rd order harmonic of 36 GHz, PAE near 36 GHz is slightly improved without increasing chip size.

3 Measured Results and Discussion

The amplifier MMIC was measured on wafer. The comparison of measured and simulated small-signal performance is shown in Fig. 5. The measured gain is 25.5 ~ 18.5 dB (comparable gain flatness to[6,7]) with less than -8.8 dB return loss at 32 ~ 40 GHz. The differences between primary-model-based simulation and measured results are caused by process variation and model error. The primary model of Win Semi is extracted with focusing on large-signal operation. Based on our experience, the gate parasitic inductor of primary model is often larger than the measured small-signal results in Ka-band. The primary model could be corrected by reducing 30% of the gate parasitic inductance. In Fig. 5, S21 and S11 of corrected-model-based simulation agree better with the measured results than those of model-based.

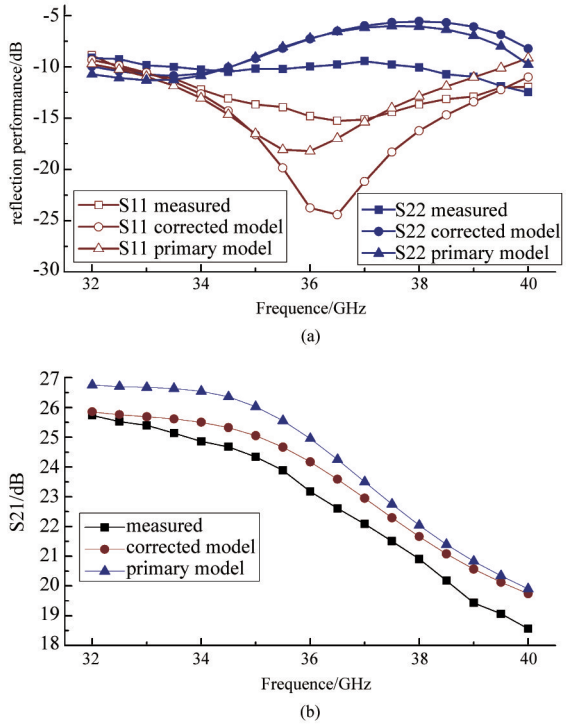

Fig. 5 (a) S11/S22 Measured and Simulated, (b) S21 Measured and Simulated
图 5 (a) S11/S22 测量与仿真,(b)S21 测量与仿真

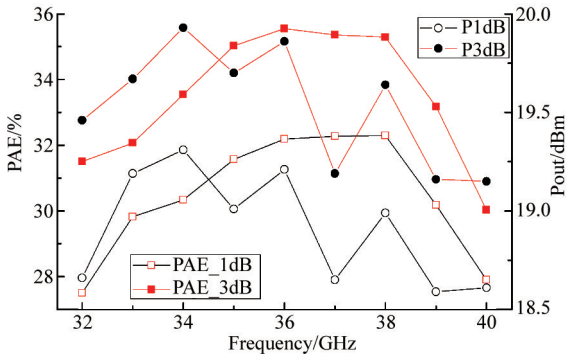

Fig. 6 Measured PAE and power
图 6 PAE 和功率测量结果

The output power and PAE (at 1 dB and 3 dB gain compression) versus frequency are shown in Fig. 6. The PAE at P_{1dB} is over 27% at 32 ~ 40 GHz with more than 18.5 dBm output power. The saturation PAE at P_{3dB} is

Table 1 Comparison of Ka-band amplifier MMIC
表 1 Ka 波段功放 MMIC 比较

Ref.	process	Stages	Output matching	Freq/GHz	Gain/dB	PAE_sat/%	Pout_sat/dBm	Size/mm
[2]	0.15μm pHEMT GaAs	1	Inductive	17 – 35	9 – 12	35 – 40	22.5 – 23.5	1.5 × 1
[5]	0.25μm pHEMT GaAs	3	Inductive	31 – 37	15 – 18	27.5	23 – 25	2.43 × 1.28
[6]	0.15μm pHEMT GaAs	3	Capacitive	30 – 38	22 – 25	20 – 36	35 – 36	3.6 × 2.75
[7]	0.15μm pHEMT GaAs	3	NA	30 – 40	14 – 20	25	33 – 34	2.8 × 2.3
[8]	0.15μm HEMT GaN	3	Inductive	26 – 33	24 – 31	28 – 35	37 – 38	3.24 × 1.74
[9]	0.15μm pHEMT GaAs	3	Inductive	33 – 48	17 – 20	20	26 – 28	2 × 1.45
[10]	pHEMT GaAs	NA	NA	34 – 42	18.5	20 – 22	20 – 21	2.4 × 1.64
This work	0.1μm pHEMT GaAs	3	Capacitive	32 – 40	18.5 – 25.5	30 – 35.5	19 – 20	2.3 × 1.5

30 ~ 35.5% with 19 ~ 20 dBm output power in 32 ~ 40 GHz.

A comparison of the Ka-band wideband PAs MMIC is shown in Table 1. The measured peak drain efficiency of final stage in our work is 46.3% at 36 GHz, which is higher than that of the single-stage PA[2] (about 44.6% at 32GHz, calculated from its data). Most medium power amplifiers are designed for linear usage as[8-9] with lower PAE about 20%. Hence, some high power amplifiers[5-7] with high PAE are listed. Accounting the losses (approximately estimated to be 1% ~3% in PAE reducing) introduced by the power combining networks in high power amplifiers, the PAE (30%-3% = 27%) of our work is still higher than the listed GaAs wideband PAs[5-6] and comparable with GaN PA[7].

Decided by the paralleling element closest to transistor, the output matching properties (capacitive /inductive) of these PAs are shown in this table. Their output matching performances can be roughly observed by S22. S22 of PA[7-8] both present only one reflection zero for the bandwidth limitation of inductive matching. However, S22 of[2] (lower operating band) and[4] (narrower operating band) both achieve two reflection zeros with inductive matching, due to the limitation of i-matching only appearing at the high operating band wideband matching (shown as Eq. (13)). Because of its multi- section capacitive matching, S22 of PA[5] presents five reflection zeros. Besides, S22 of our work has two reflection zeros (One is 33.5 GHz, the other is higher than 40 GHz.) with capacitive matching.

4 Conclusion

This paper presents a Ka-band high efficiency three-stage wideband PA MMIC with capacitive coupled matching structure. A set of formulas was proposed to calculate initial values of this matching and facilitate the optimization process. With the correcting of the frequency offset, these formulas are more accurate than those presented in Ref. [2]. The measured PAE of this PA is higher than 30% over the entire frequency band (32 ~ 40 GHz). These results demonstrate the effectiveness of this design method for millimeter wave wideband PA.

References

[1] TANG Kan, FU Kun, SUN Xian, *et al*. Signature analysis and 3-D reconstruction of rectangular building in very high resolution SAR images [J]. *J. Infrared Millim. Waves*(唐侃, 付琨, 孙显等. 高分辨率 SAR 图像中矩形建筑物特性分析与三维重建. **红外与毫米波学报**), 2013, **32**(3): 198 – 204.

[2] Huang P-C, Tsai Z-M, Lin K-Y, *et al*. A 17 – 35 GHz Broadband, High Efficiency PHEMT Power Amplifier Using Synthesized Transformer Matching Technique [J]. *IEEE Transactions on Microwave Theory and Techniques*, 2012, **60**(1): 112 – 119.

[3] YANG Ge-Liang, WANG Zhi-Gong, LI Zhi-Qun, *et al*. Millimeter-wave Low Power UWB CMOS Common-gate LNA [J]. *J. Infrared Millim. Waves*(杨格亮, 王志功, 李智群等. CMOS 毫米波低功耗超宽带共栅低噪声放大器. **红外与毫米波学报**), 2014, **33**(6): 584 – 590.

[4] Huang C W, Chang S J, Wu W, *et al*. Chang. A Three-Stage Ka Band PHEMT Wideband Amplifier MMIC [J]. *Microwave and Optical Technology Letters*, 2004, **42**(4): 277 – 280.

[5] Campbell C F, Dumka D C, Kao M-Y, *et al*. Design and Performance of a High Efficiency Ka-band Power Amplifier MMIC [C]. 2010 IEEE Compound Semiconductor Integrated Circuit Symposium. Monterey, CA, 2010: 1 – 4.

[6] TGA4516 Datasheet[R]. Oregon: TriQuint Semi, 2011.

[7] Campbell C F, Liu Y, Kao M-Y, *et al*. High Efficiency Ka-Band Gallium Nitride Power Amplifier MMICs[C]. 2013 IEEE International Conference on Microwaves, Communications, Antennas and Electronics Systems. Tel Aviv, 2013: 1 – 5.

[8] Chen S, Nayak S. A 1/2 Watt High Linearity and Wide Bandwidth PHEMT Driver Amplifier MMIC for Millimeter-Wave Applications [C]. IEEE MTT-S International Microwave Symposium Digest. San Francisco, CA, 2006: 1863 – 1866.

[9] HMC-ABH264 Datasheet [R]. Massachusetts: Hittite Microwave Corp, 2015.

[10] 0.1um GaAs PHEMT Device Model Handbook [R]. Taiwan: WIN Semiconductors Corp, 2013.

(上接 528 页)

[16] Liu J, Xiao M, Shen J, *et al*. Flexible PMMA pipe for terahertz propagation[C]. *Photonics Asia. International Society for Optics and Photonics*, Beijing, 2012: 85620R – 85620R – 7.

[17] Xiao M, Liu J, Zhang W, *et al*. THz wave transmission in thin-wall PMMA pipes fabricated by fiber drawing technique[J]. *Optics Communications*, 2013, **298**: 101 – 105.

[18] Xiao M, Liu J, Zhang W, *et al*. Self-supporting polymer pipes for low loss single-mode THz transmission. [J]. *Optics Express*, 2013, **21**(17): 19808 – 19815.

[19] You B, Lu J Y, Yu C P, *et al*. Terahertz refractive index sensors using dielectric pipe waveguides[J]. *Optics Express*, 2012, **20**(6): 5858 – 66.

[20] Centini M, Sibilia C, Scalora M, *et al*. Dispersive properties of finite, one-dimensional photonic band gap structures: applications to nonlinear quadratic interactions. [J]. *Physical Review E*, 1999, **60**(4): 4891.